

Research on Pneumothorax Detection Based on Magneto-Acousto-Electrical Tomography

Cailian Li^{1, 2}, Yuanyuan Li^{1, *}, and Guoqiang Liu^{1, 2, *}

Abstract—Pneumothorax can cause chest tightness, chest pain, and respiratory failure, which can be life-threatening in severe cases. Therefore, early diagnosis and treatment of pneumothorax are crucial. Magneto-Acousto-Electrical Tomography (MAET) is an imaging technique in which ultrasound and electromagnetism are mutually coupled. It has the advantages of high spatial resolution and high image contrast. In this paper, we use MAET to study porous and air-containing lung tissue. We first simulate the characteristics of the MAET signal as the degree of pneumothorax increases. The relationship between the size of the ultrasonic probe and the size of the pneumothorax was discussed. The simulation results show that the reflection and attenuation values of the MAET voltage signals increase as the pneumothorax size gradually increases, regardless of whether the ultrasound transducer size is larger or smaller than the pneumothorax size. Finally, the MAET experimental platform was built to validate the simulation results of MAET signals. The results of the experiment and simulation are consistent with each other. The research of this paper has a certain reference value for the detection of pneumothorax using MAET.

1. INTRODUCTION

Pneumothorax is a respiratory disease caused by gas entering the pleural cavity. It can cause symptoms such as chest pain, chest tightness, and difficulty in breathing. In severe cases, it can cause acute respiratory failure and endanger the patient's life [1–3]. The main diagnostic methods of pneumothorax include CT and ultrasound imaging [4, 5].

CT is the primary diagnosis of pneumothorax. However, it is expensive and radioactive. It is not suitable for children and pregnant women. Lung ultrasound of pneumothorax is characterized by low radiation and high operability, but its spatial resolution is low. Therefore, it is crucial to explore new imaging methods to detect pneumothorax. MAET is an imaging technology coupled electromagnetic and ultrasonic field [6–8], which has the advantages of high spatial resolution of ultrasonic imaging and high contrast of electrical impedance tomography (EIT).

In 1998, Han et al. studied the charge separation of charged ions under Lorentz force in the static magnetic field. This phenomenon is called Hall Effect Imaging (HEI) technology [9]. MAET is Hall Effect imaging based on electrical signal detection. Haider et al. derived the relationship between surface voltage and reciprocity current density and equivalent source electric field strength based on the reciprocity theorem formula [10]. Zeng et al. studied the coupling process of sound field and electromagnetic field. The current density of copper was reconstructed [11]. Graslandmongrain from France used a focused ultrasound transducer to measure beef samples and performed B-scan imaging [12]. Guo et al. used the time-reversal method to reconstruct the conductivity of MAET [13]. A novel simulation model of a coil structure was developed by Zengin and Gençer, in Turkey.

Received 28 August 2021, Accepted 24 November 2021, Scheduled 7 December 2021

* Corresponding authors: Yuanyuan Li (lyy@mail.iee.ac.cn), Guoqiang Liu (gqliu@mail.iee.ac.cn).

¹ Institute of Electrical Engineering, Chinese Academy of Sciences, Beijing, China. ² University of Chinese Academy of Sciences, Beijing, China.

The feasibility of coil structures to detect MAET signals was investigated, but no experimental verification was performed [14]. Kunyansky et al. of the University of Arizona proposed a method for reconstructing the conductivity distribution by current density vector, which was validated by simulation [15]. A noninvasive method of treatment-efficacy evaluation for HIFU ablation using the MAET was theoretically studied by Zhou et al. The relevant model was established to prove the feasibility of real-time evaluation of HIFU treatment effect by the MAET [16]. Yu et al. used sine-Barker coded excitation and obtained clear MAET signals from triple-layer animal gel simulations [17]. Li et al. simulated a biological tissue model and reconstructed the electrical characteristics, reflecting the physiological or pathological state. The axial resolution of 1 mm was obtained by correlation imaging experiments on the phantom and pork tissue samples [18]. Dai et al. designed and implemented an MAET system with a chirp pulse stimulation (MAET-CPS) method based on the Verasonics system and MC600 displacement platform. A focal probe was utilized for steps that can focus excitation on enhancing the imaging resolution [19]. Sun et al. applied pulse compression technology in MAET and proved its feasibility through simulated experiments [20].

All of the above MAET research references are aimed at gel phantoms of low salinity solid [17–20] or from animal tissue samples [12, 18, 19]. No relevant research has been carried out on lung tissue that is porous and contains air.

In this study, the principle of MAET was introduced, and then a simulation model was established. The signal characteristics of MAET were simulated according to the degree of pneumothorax. The relationship between the size of the ultrasonic probe and the size of the pneumothorax was studied. Finally, the experimental verification was carried out.

2. PRINCIPLE AND METHOD

The principle of MAET is shown in Fig. 1. The target sample is excited by ultrasound, which triggers the vibration of positive and negative ions within the target sample. Under the static magnetic field, the ions are separated by Lorentz force. It will result in a current distribution that varies with the propagation of the ultrasound. The corresponding MAET signal can be detected by the electrode.

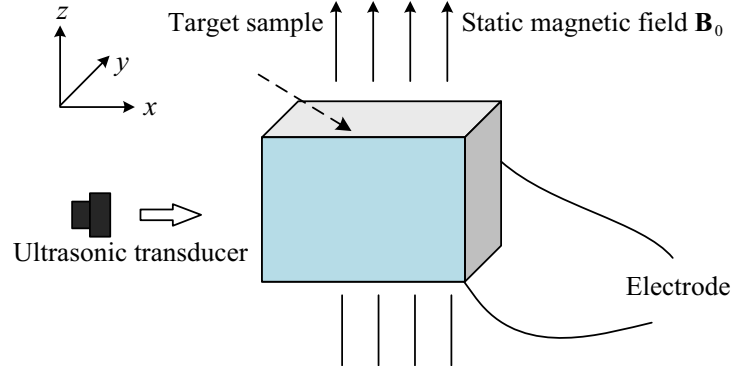


Figure 1. Schematic diagram of MAET.

It is assumed that the ultrasonic wave generated by the ultrasonic transducer propagates along the \mathbf{e}_x direction. The static magnetic field is along the \mathbf{e}_z direction. The magnitude of the static magnetic field is \mathbf{B}_0 .

The effects of viscosity and nonlinearity are not considered to simplify the theoretical derivation. The particle velocity satisfies the equation of motion in a homogeneous ideal fluid medium.

$$\rho_0 \frac{\partial v(x, t)}{\partial t} + \frac{\partial p(x, t)}{\partial x} = 0 \quad (1)$$

where ρ_0 is the density of the target sample, and $p(x, t)$ is the ultrasonic pressure along the \mathbf{e}_x direction.

From Equation (1), the equation of particle velocity is obtained as follows

$$v(x, t) = -\frac{1}{\rho_0} \int_{-\infty}^t \frac{\partial p(x, t)}{\partial x} dt \tag{2}$$

Under the static magnetic field, the positive and negative ions are affected by the Lorentz force

$$\mathbf{F} = q\mathbf{v} \times \mathbf{B}_0 \tag{3}$$

Under the Lorentz force, charge separation occurs between positive and negative ions, resulting in an equivalent current source

$$\mathbf{J}_e = \sigma\mathbf{v} \times \mathbf{B}_0 \tag{4}$$

where σ is the conductivity of the target sample, and \mathbf{J}_e is the current density of the equivalent current source.

According to Ohm's law, the conduction current in the target sample is

$$\mathbf{J}_o = -\sigma\nabla u \tag{5}$$

Substituting Equation (5) into the generalized Ohm's law, the total current density in the target sample is

$$\mathbf{J}_T = \sigma\mathbf{v} \times \mathbf{B}_0 - \sigma\nabla u \tag{6}$$

According to the principle of continuity of electric current, Poisson's equation for the standard electric position of the target sample can be derived

$$\nabla \cdot (\sigma\nabla u) = \nabla \cdot (\sigma\mathbf{v} \times \mathbf{B}_0) \tag{7}$$

According to Equation (7), the electrode can detect the voltage signal u using the MAET method. Since MAET is excited by ultrasound, and the vibration velocity in Equation (7) comes from the MAET excitation ultrasonic signal, and MAET has the advantage of the high spatial resolution of ultrasonic technology. The MAET voltage signal obtained from Equation (7) contains the electrical properties. For biological tissue, the electrical conductivity change of electrical conductivity was earlier than that of tissue structure. Thus, the conductivity of biological tissue has the advantages of high image contrast.

3. NUMERICAL STUDIES

The simulation model is shown in Fig. 2. The size of the gray part of the model is $(1.2 \times 1.4) \text{ cm}^2$ and conductivity set to 0.2 S/m . The rectangle next to the blue section simulates lung tissue that is porous and contains air. The size is $(0.5 \times 0.8) \text{ cm}^2$, and the conductivity is set to 0.15 S/m . The blue part simulates pneumothorax, and the material is set as air. $d2$ denotes the y -direction pneumothorax size, and h denotes the x -direction pneumothorax size.

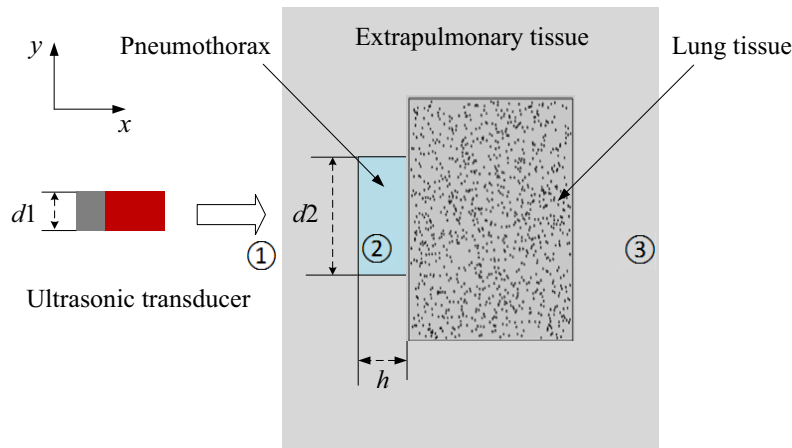


Figure 2. Schematic diagram of the pneumothorax simulation model.

As the degree of pneumothorax increases, the intrathoracic gas content gradually increases. Therefore, a simulation study was performed to simulate the gradual increase of the gas content in the chest cavity as h changed from (0.1, 0.2, 0.3, 0.4) cm.

The relative size of ultrasonic transducer $d1$ and pneumothorax $d2$ will affect the MAET signal. Therefore, the simulation investigates the characteristics of the MAET signal during the gradual increase of the pneumothorax size h when the size of the ultrasonic transducer $d1$ is larger and smaller than the pneumothorax size $d2$.

3.1. $d1 < d2$

A simulation study was performed where the ultrasound transducer size $d1$ was smaller than the pneumothorax size $d2$. The simulation was set to $d1 = 0.4$ cm and $d2 = 0.8$ cm. The pneumothorax size h was gradually changed from (0.1, 0.2, 0.3, 0.4) cm to simulate the increase of the degree of pneumothorax lesion. The simulation results are shown in Fig. 3.

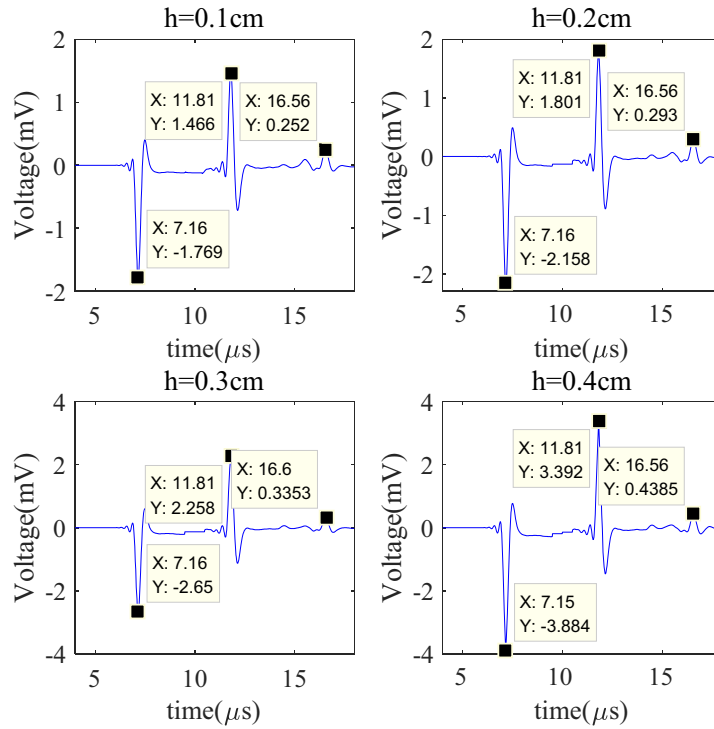


Figure 3. MAET signals with $d1$ less than $d2$.

According to the simulation results in Fig. 3, when the ultrasonic transducer size $d1$ is smaller than the pneumothorax size $d2$, three MAET pulse signals are generated under different sizes of h . The first negative MAET pulse signal 1 is generated when ultrasound propagates to the boundary ① of extrapulmonary tissue. The second positive MAET pulse signal 2 was generated by ultrasound propagating to the boundary ② of pneumothorax and then reflecting the boundary ① of extrapulmonary tissue. The third positive MAET pulse signal 3 is generated when the ultrasound bypasses the pneumothorax and lung tissue. Then ultrasound propagates to the boundary ③ of extrapulmonary tissue.

According to the above simulation results, the sound energy reflection percentage R is calculated as follows

$$R = \frac{A2}{A1} \quad (8)$$

where $A1$ is the amplitude of MAET pulse signal 1 produced by ultrasound propagating to the boundary

① of extrapulmonary tissue, and A_2 is the amplitude of MAET pulse signal 2 generated by sound energy reflection.

Then calculate the attenuation percentage D

$$D = \frac{|A_1 - A_3|}{A_1} \tag{9}$$

where A_3 is the amplitude of MAET pulse signal 3.

Plot R and D curves as shown in Fig. 4.

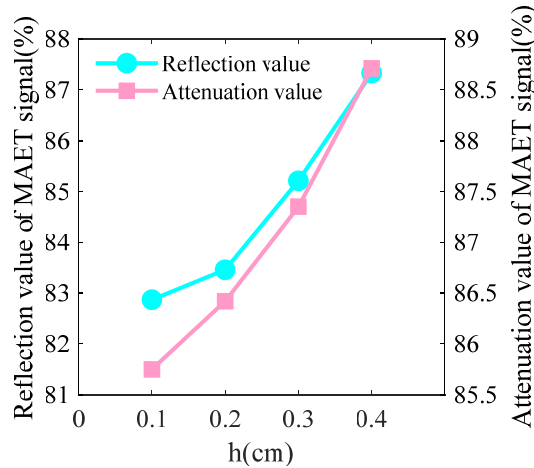


Figure 4. Simulation results of R and D curves with d_1 less than d_2 .

From the results in Fig. 4, it is clear that when $d_1 < d_2$, the MAET voltage signal reflection and attenuation values increase as the pneumothorax size h gradually increases.

3.2. $d_1 > d_2$

Simulation analysis was performed when the ultrasound transducer size d_1 was larger than the pneumothorax size d_2 .

It can be seen from the simulation results in Fig. 5 that when d_1 is greater than d_2 , three MAET pulse signals are still generated for different h .

The first negative MAET pulse signal 1 is generated when ultrasound propagates to the boundary ① of extrapulmonary tissue. The second positive MAET pulse signal 2 is generated when the ultrasound propagates to the boundary ② of pneumothorax and then reflects the boundary ① of extrapulmonary tissue. The third positive MAET pulse signal 3 is generated by ultrasound passing through pneumothorax and lung tissue to the boundary ③ of extrapulmonary tissue. Calculate R and D according to formula (8) and formula (9), and draw the curves of R and D as shown in Fig. 6.

From the results in Fig. 6, it can be seen that when d_1 is larger than d_2 , the MAET voltage pulse signal reflection and attenuation values increase with the gradual increase of pneumothorax size h . However, when d_1 is smaller than d_2 , both the reflection and attenuation values of the MAET voltage pulse signal are larger than those when d_1 is larger than d_2 .

3.3. Comparison of MAET Signals between Pneumothorax and Normal Lung

When $d_1 < d_2$, the normal lung was simulated by MAET. The MAET signals of normal lung and lung with pneumothorax ($h = 0.1$ cm) were compared, and the results are shown in Fig. 7.

From Fig. 7, we can see that during pneumothorax, the MAET signal generated by reflected ultrasound propagating to lung tissue ① appears in $11.81 \mu\text{s}$, while the MAET signal generated by reflected ultrasound propagating to normal lung appears in $13.11 \mu\text{s}$. Compared with normal lung, the MAET signal produced by reflected ultrasound appears earlier in pneumothorax. During pneumothorax,

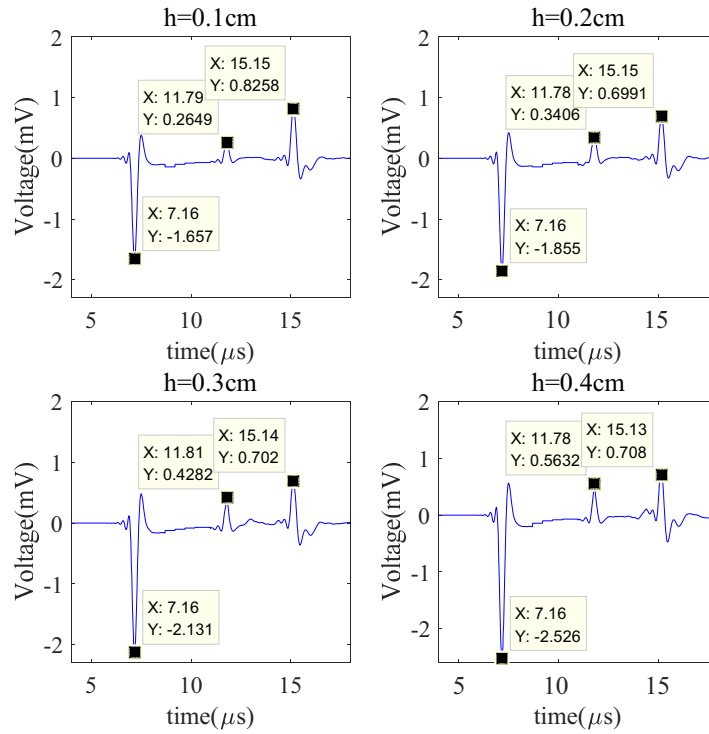


Figure 5. MAET signal with $d1$ greater than $d2$.

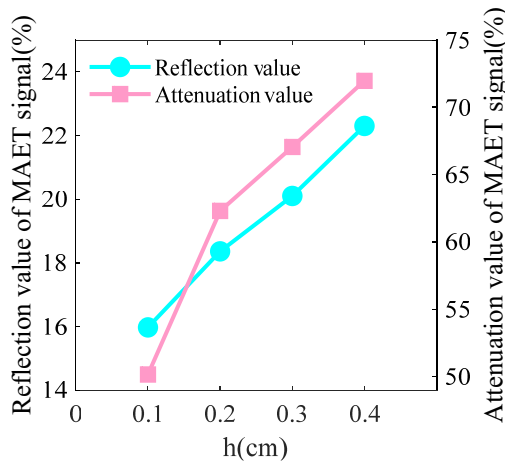


Figure 6. Simulation results of R and D curves with $d1$ greater than $d2$.

the reflection value of the MAET voltage signal is 82.8%, and the attenuation value is 85.8%. The reflection value of the MAET voltage signal in the normal lung is 79.4%, and the attenuation value is 80.34%. The reflection value and attenuation value of the MAET voltage signal during pneumothorax are greater than those of normal lung.

4. EXPERIMENTAL VERIFICATION

The following experimental verification of the pneumothorax is performed. The schematic diagram of the experimental system is shown in Fig. 8. It includes an ultrasonic transducer, movement control device of the ultrasonic transducer, permanent magnet, signal generator, measurement electrode, signal

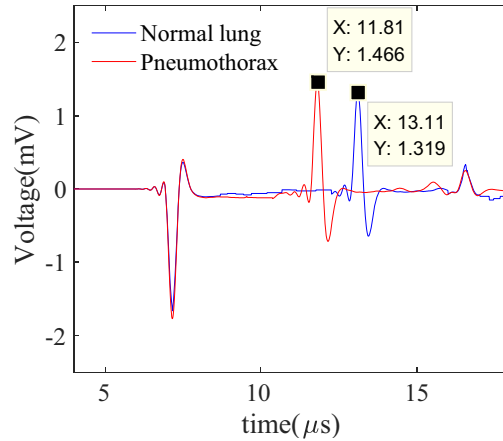


Figure 7. MAET simulation signals of pneumothorax and normal lung.

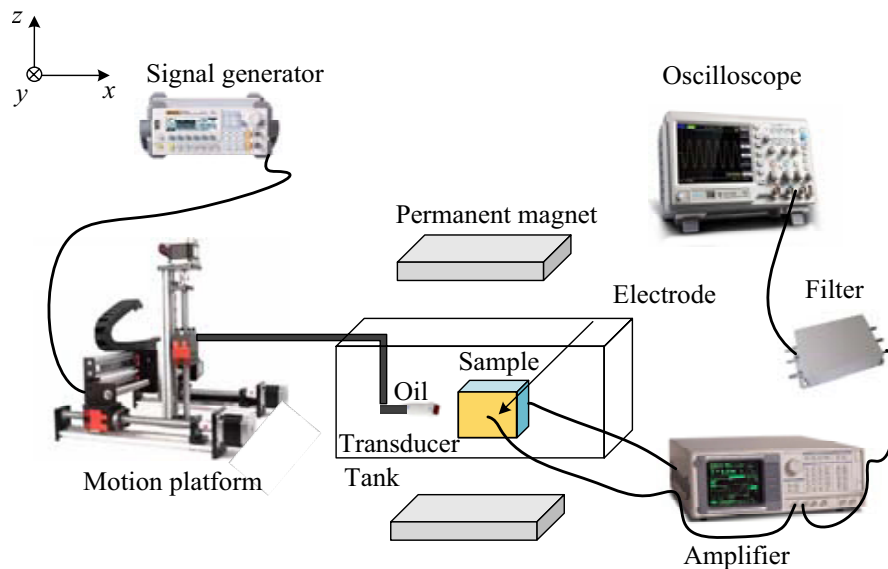


Figure 8. Schematic diagram of MAET experimental system.

amplifier, signal filter, and oscilloscope.

The permanent magnets are two pieces of NdFeB of size $(30 \times 30 \times 10) \text{ cm}^3$. A static magnetic field of 300 mT can be generated in the middle 6 cm cube area. An oil tank of size $(30 \times 12 \times 9) \text{ cm}^3$ is placed in the gap between the two permanent magnets. The tank is filled with transformer oil, and the ultrasonic transducer and the experimental phantom are submerged in the transformer oil.

During the experiment, the phantom was placed in the static magnetic field generated by the permanent magnet. The excitation source of the ultrasonic transducer is a pulse signal, which is generated by the signal generator and amplified by the power amplifier. Then a pair of electrodes are then used to detect the MAET signal, which is amplified, filtered, and displayed on the oscilloscope.

In the experiment, the phantom was composed of gel powder and water. NaCl was added to simulate the conductivity of biological tissue. The phantom size of the simulated extrapulmonary tissue is $(7.5 \times 5 \times 5) \text{ cm}^3$, and the conductivity is 0.2 S/m. A black polyurethane sponge was used to simulate lung tissue. The polyurethane sponge is filled with gel phantom with conductivity. Its size is $(2 \times 1 \times 5) \text{ cm}^3$, and its conductivity is 0.15 S/m. A hole with the size of h was made inside the phantom to simulate pneumothorax. The distance between the front boundary of pneumothorax and the mimicry front boundary of extrapulmonary tissue was 1 cm.

4.1. $d1 < d2$

The MAET signal is first studied when the ultrasonic transducer size $d1$ is smaller than the pneumothorax size $d2$. The ultrasonic transducer size $d1$ is 1.3 cm, and the pneumothorax size $d2$ is 2 cm. The pneumothorax size h varies from (0.5, 1, 1.5, 2) cm to simulate the gradual increase of gas in the chest cavity. The physical diagram of the phantom is shown in Fig. 9, and the experimental results are shown in Fig. 10.

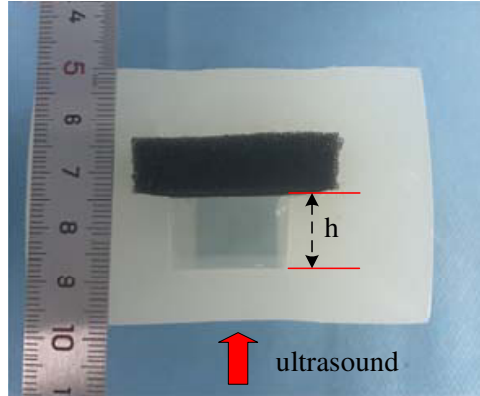


Figure 9. Phantom diagram with $d1$ less than $d2$.

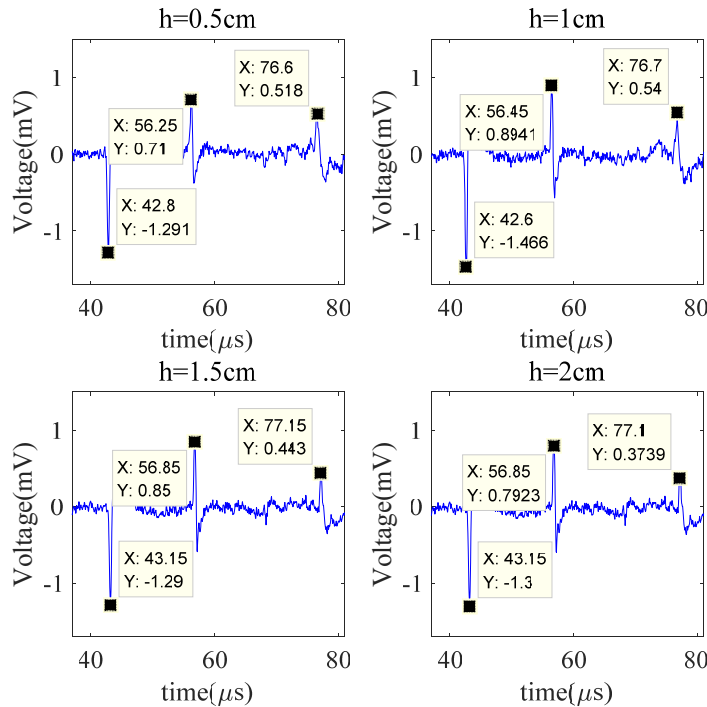


Figure 10. Experimental results with $d1$ less than $d2$.

It can be seen from the experimental results in Fig. 10 that when the ultrasonic transducer size $d1$ is less than the pneumothorax size $d2$, three MAET pulse signals are generated under different sizes of h . The signal is consistent with the simulation results when $d1$ is less than $d2$, not repeated here. Calculate R and D according to formula (8) and formula (9), and draw the curve of R and D as shown in Fig. 11.

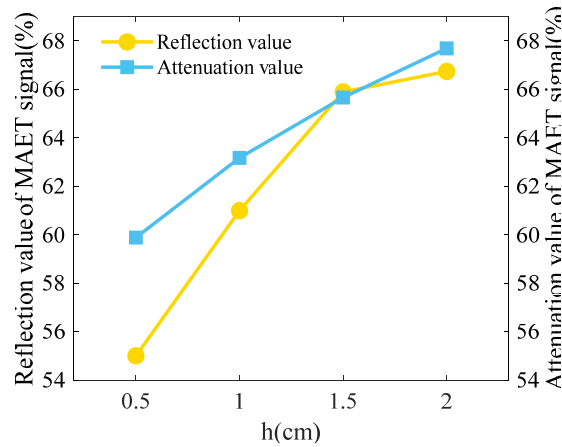


Figure 11. Experimental results of R and D curves with $d1$ less than $d2$.

It can be seen from the experimental results in Fig. 11 that when $d1$ is less than $d2$, the reflection and attenuation values of the MAET voltage signal increase with the increase of pneumothorax size h .

4.2. $d1 > d2$

The MAET signals of the ultrasonic transducer size $d1$ larger than the pneumothorax size $d2$ were studied. The ultrasonic transducer size $d1$ is 1.3 cm, and the pneumothorax size $d2$ is 0.5 cm. The pneumothorax size h varies from (0.5, 1, 1.5, 2) cm to simulate the gradual increase of gas in the chest cavity. The phantom diagram of the experiment is shown in Fig. 12, and the results are shown in Fig. 13.

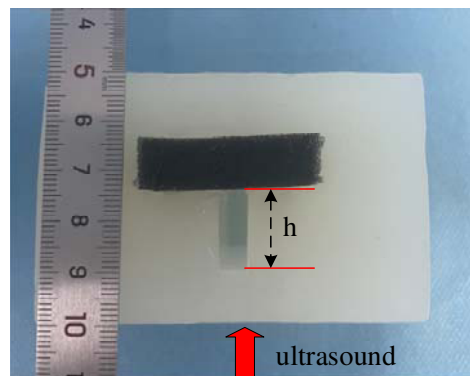


Figure 12. Experimental phantom diagram with $d1$ greater than $d2$.

It can be seen from the experimental results in Fig. 13 that when $d1$ is greater than $d2$, three MAET pulse signals are still generated under different sizes of h . The signal is consistent with the simulation results when $d1$ is greater than $d2$, not repeated here. Calculate R and D according to formula (8) and formula (9), and draw the curve of R and D as shown in Fig. 14.

According to the experimental results in Fig. 14, when $d1$ is greater than $d2$, the values of reflection and attenuation for the MAET voltage signal increase with pneumothorax size h .

4.3. Comparison of MAET Experimental Signals between Pneumothorax and Normal Lung

When $d1 < d2$, MAET was performed on normal lungs. The MAET signals of normal lung and lung with pneumothorax ($h = 0.5$ cm) were compared, and the results are shown in Fig. 15.

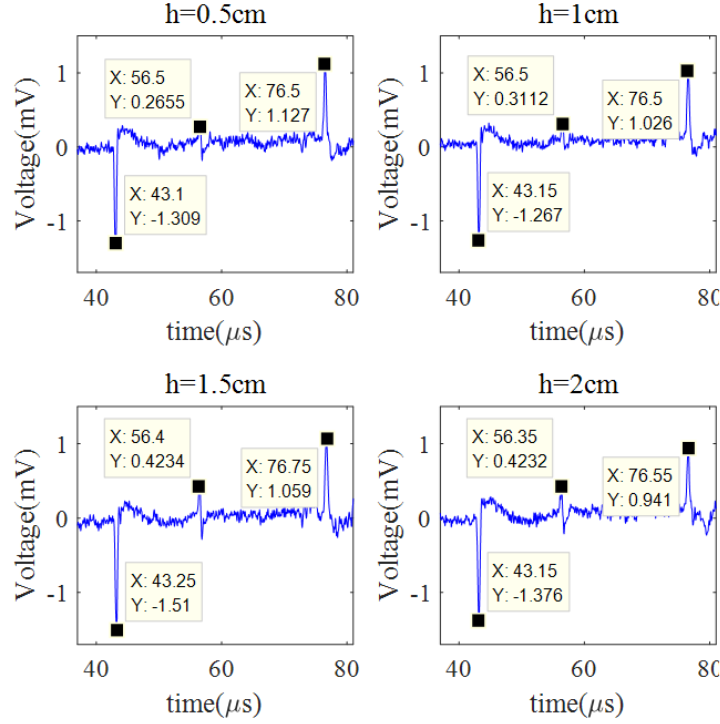


Figure 13. Experimental results of R and D curves with $d1$ greater than $d2$.

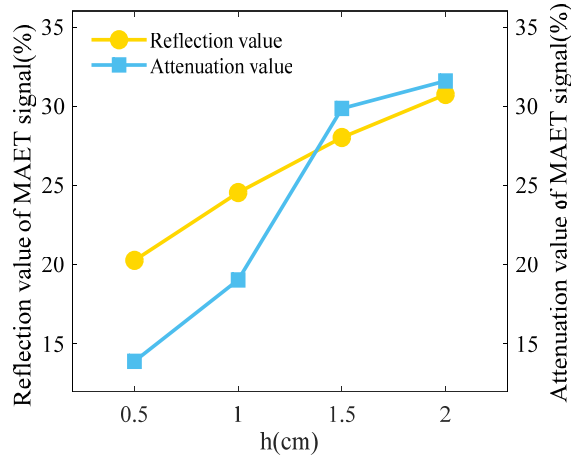


Figure 14. Experimental results of R and D curves with $d1$ greater than $d2$.

From Fig. 15, we can see that during pneumothorax, the MAET signal generated by reflected ultrasound propagating to lung tissue ① appears in $56.25\ \mu\text{s}$, while the MAET signal generated by reflected ultrasound propagating to normal lung appears in $62.75\ \mu\text{s}$. Compared with normal lung, the MAET signal produced by reflected ultrasound appeared earlier in pneumothorax. During pneumothorax, the reflection value of the MAET voltage signal is 55%, and the attenuation value is 59.9%. The reflection value of the MAET voltage signal in normal lung tissue is 53.6%, and the attenuation value is 46.4%. The reflection value and attenuation value of the MAET voltage signal during pneumothorax are greater than those of normal lung. The experimental results are consistent with the simulation ones.

From the above experimental results, it is clear that with the increase of pneumothorax size h , the reflection and attenuation values of the MAET voltage signal increase no matter $d1$ is larger or smaller

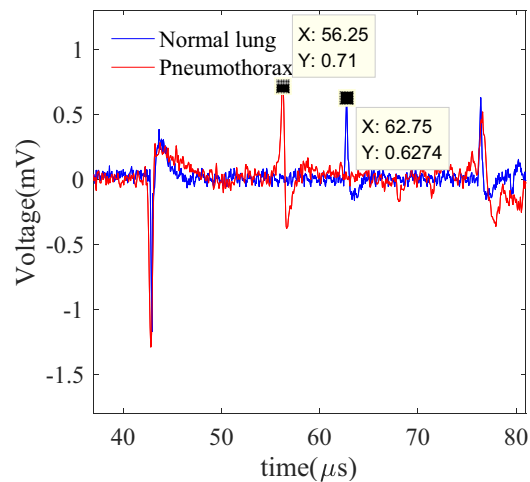


Figure 15. MAET experimental signals of pneumothorax and normal lung.

than $d2$. When $d1$ is less than $d2$, the reflection and attenuation of the MAET voltage signal are larger than when $d1$ is greater than $d2$. The occurrence time of the MAET signal generated after ultrasound transmission to pneumothorax reflection is earlier than that generated after ultrasound transmission to normal lung reflection. The reflection value and attenuation value of the MAET voltage signal during pneumothorax are greater than those of normal lung. The experimental results are consistent with the previous simulated ones.

5. CONCLUSION

MAET has the advantages of high spatial resolution and high contrast. In this paper, we used MAET to detect pneumothorax in porous lung tissue. The simulation model was established to study the characteristics of MAET signals with the increasing degree of pneumothorax. The relationship between the size of the ultrasonic probe and the size of the pneumothorax was studied. The difference of MAET signals between pneumothorax and normal lung was studied and analyzed. Finally, the MAET experimental platform was built and verified by relevant experiments. In the experiment, the per-lung tissue was simulated by phantom; the polyurethane sponge simulated the normal lung; and the pneumothorax was simulated by air.

Although there are differences between the simulation method and the actual pneumothorax, we can still get the relevant conclusions: With the increase of pneumothorax size h , the reflection and attenuation values of MAET voltage signal increase no matter the size of the ultrasonic transducer is larger or smaller than pneumothorax size. When the ultrasonic transducer is smaller than the size of pneumothorax, the reflection and attenuation of the MAET voltage signal are larger than that when the ultrasonic transducer is larger than the size of the pneumothorax. The occurrence time of the MAET signal generated after ultrasound transmission to pneumothorax reflection is earlier than that generated after ultrasound transmission to normal lung reflection. The reflection value and attenuation value of the MAET voltage signal during pneumothorax are greater than those of normal lung. The research results of this paper have a certain reference value for the detection of pneumothorax by MAET.

ACKNOWLEDGMENT

This work was supported by the National Natural Science Foundation of China (NNSFC) under Grant No. 51937010 and the Youth Science Foundation Project under Grant No. 52007182.

REFERENCES

1. Baumann, M. H. and C. Strange, "The clinician's perspective on pneumothorax management," *CHEST*, Vol. 112, No. 3, 822–828, 1997.
2. Seremetis, M. G., "The management of spontaneous pneumothorax," *CHEST*, Vol. 57, No. 1, 65–68, 1970.
3. Tschopp, J. M., R. Rami-Porta, M. Noppen, et al., "Management of spontaneous pneumothorax: State of the art," *European Respiratory Journal*, Vol. 28, No. 3, 637, 2006.
4. Volpicelli, G., M. Elbarbary, M. Blaivas, et al., "International evidence-based recommendations for point-of-care lung ultrasound," *Intensive Care Medicine*, Vol. 38, No. 4, 577–591, 2012.
5. Wernecke, K., M. Galanski, P. E. Peters, et al., "Pneumothorax: Evaluation by ultrasound—preliminary results," *Journal of Thoracic Imaging*, Vol. 2, No. 2, 76–78, 1987.
6. Li, Y., J. X. Song, et al., "Three-dimensional model of conductivity imaging for Magneto-Acousto-Electrical Tomography," *Journal of Applied Physics*, Vol. 127, No. 10, 104701, Mar. 2020.
7. Kaboutari, K., A. O. Tetik, et al., "Data acquisition system for MAET with magnetic field measurements," *Physics in Medicine & Biology*, Vol. 64, 110516, 2019.
8. Li, Y., J. X. Song, et al., "The experimental study of mouse liver in Magneto-Acousto-Electrical Tomography by scan mode," *Physics in Medicine and Biology*, Vol. 65, No. 21, 215024, 2020.
9. Han, W., S. Jatin, and S. Robert, "Hall effect imaging," *IEEE Transactions on Biomedical Engineering*, Vol. 45, No. 1, 119–124, 1998.
10. Haider, S., A. Hrbek, and Y. Xu, "Magneto-Acousto-Electrical Tomography: A potential method for imaging current density and electrical impedance," *Physiological Measurement*, Vol. 29, No. 6, S41–50, 2008.
11. Zeng, X., G. Liu, H. Xia, et al., "An acoustic characteristic study of Magneto-Acousto-Electrical Tomography," *International Conference on Biomedical Engineering and Informatics*, 95–98, 2010.
12. Graslandmongrain, P., J. M. Mari, J. Y. Chapelon, et al., "Lorentz force electrical impedance tomography," *IRBM*, Vol. 34, No. 4, 357–360, 2013.
13. Guo, L., G. Liu, and H. Xia, "Magneto-Acousto-Electrical Tomography with magnetic induction for conductivity reconstruction," *IEEE Transactions on Biomedical Engineering*, Vol. 62, No. 9, 2114–2124, 2015.
14. Zengin, R. and N. G. Gençer, "Lorentz force electrical impedance tomography using magnetic field measurements," *Physics in Medicine & Biology*, Vol. 61, No. 16, 5887–5905, 2016.
15. Kunyansky, L., C. P. Ingram, and R. S. Witte, "Rotational Magneto-Acousto-Electric Tomography (MAET): Theory and experimental validation," *Physics in Medicine & Biology*, Vol. 62, No. 8, 3025, 2017.
16. Zhou, Y., Z. Yu, Q. Ma, et al., "Noninvasive treatment-efficacy evaluation for HIFU therapy based on Magneto-Acousto-Electrical Tomography," *IEEE Transactions on Biomedical Engineering*, Vol. 66, No. 3, 666–674, 2019.
17. Yu, Z. F., Y. Zhou, Y. Z. Li, Q. Y. Ma, G. P. Guo, and J. Tu, "Performance improvement of Magneto-Acousto-Electrical Tomography for biological tissues with sinusoid-Barker coded excitation," *Chinese Physics B*, Vol. 27, No. 9, 094302, 2018.
18. Li, Y., G. Liu, et al., "Numerical simulations and experimental study of Magneto-Acousto-Electrical Tomography with plane transducer," *IEEE Transactions on Magnetics*, Vol. 54, No. 3, 1–4, 2018.
19. Dai, M., X. Chen, T. Sun, et al., "A 2D Magneto-Acousto-Electrical Tomography method to detect conductivity variation using multifocus image method," *Sensors*, Vol. 18, No. 7, 2231, 2018.
20. Sun, Z. S., G. Q. Liu, and H. Xia, "Lorentz force electrical impedance tomography using pulse compression technique," *Chinese Physics B*, Vol. 26, No. 12, 124302, 2017.